Continuum Modeling of Micro-particle Electrorotation in Couette and Poiseuille Flows—the Zero Spin Viscosity Limit

Hsin-Fu Huang, Markus Zahn, *Fellow, IEEE*, Elisabeth Lemaire, and Mark I. Shliomis

***Abstract*—A continuum mechanical model is developed to analyze the electrorheological responses and flow phenomena of a particle-liquid mixture with the suspended micro-particles undergoing spontaneous electrorotation, or Quincke rotation, for both two dimensional Couette and Poiseuille flow geometries by combining particle electromechanics and continuum anti-symmetric stress analyses in the zero spin viscosity limit. Predicted results show that with a direct current electric field strength higher than the Quincke threshold applied perpendicularly to the flow direction, the spin velocity is increased and the effective viscosity is decreased as compared to the zero electric field value of the electrorheological fluid viscosity for Couette flow at a given driving shear rate. Moreover, it is also found that with a constant driving pressure gradient, the spontaneous internal particle electrorotation increases the electrorheological fluid rotation as well as enhances the flow velocity and the subsequent two-dimensional volume flow rate of Poiseuille flow when the applied direct current electric field perpendicular to the direction of flow has a strength higher than the critical strength for the onset of Quincke rotation. These continuum mechanical results of the effective viscosity and volume flow rate qualitatively agree with those obtained from effective continuum models (based on single particle dynamics) and general experimental observations as found in current literature.**

***Index Terms*—Continuum anti-symmetric stress tensor; electrohydrodynamics; Maxwell-Wagner polarization; negative electrorheology; Quincke rotation**

H.-F. Huang is financially supported by the National Science Council (Taipei, Taiwan) through the Taiwan Merit Scholarships under grant no. TMS-094-2-A-029. This work was supported in part by the United States-Israel Binational Science Foundation (BSF) through grant no. 2004081.

Hsin-Fu Huang is with the Department of Mechanical Engineering at the Massachusetts Institute of Technology, Cambridge, MA 02139 USA (e-mail: hfthuang@mit.edu).

Markus Zahn is with the Laboratory for Electromagnetic and Electronic Systems of the Department of Electrical Engineering and Computer Science at the Massachusetts Institute of Technology, Cambridge, MA 02139 USA (phone: 617-253-4688; fax: 617-258-6774; e-mail: zahn@mit.edu).

Elisabeth Lemaire is with the Laboratoire de Physique de la Matière Condensée, CNRS, at the Université de Nice, Parc Valrose, 06108 Nice cedex 2, France.

Mark I. Shliomis is with the Department of Mechanical Engineering at the Ben-Gurion University of the Negev, P.O. Box 653 Beer-Sheva 84105, Israel.

I. INTRODUCTION

ELECTRORHEOLOGICAL (ER) fluids are a class of fluids that consist of conducting or insulating solid micro-particles suspended within a dielectric liquid medium. Due to the electrical property (*e.g.* conductivity and/or permittivity) mismatch between the solid and liquid phases, one can control the apparent macroscopic properties of the ER fluid such as the bulk modulus or the effective viscosity via the application of external electric fields. Literature has therefore categorized ER effects, based on the flow or rheological responses, into either positive ER or negative ER phenomena when the fluid is subjected to electric fields [1]-[6].

Foulc *et al.* [4] and Boissy *et al.* [5] had their first qualitative distinction of the positive and negative ER effects based upon the relative magnitudes of the respective electrical conductivities of the solid and liquid phases. For ER fluids consisting of micro-particles with a conductivity, σ_2, larger than that, σ_1, of the carrier liquid, stable particle chains are formed in the direction of the electric field so that the macroscopic fluid resistance against externally applied shear perpendicular to the electric field is enhanced and result in an increased measured modulus or effective viscosity—the positive ER effect [1]-[3]. On the other hand, when the conductivity of the carrier liquid is larger than that of the micro-particles, *i.e.*, $\sigma_1 > \sigma_2$, laminated layers (perpendicular to the electric field) of packed particles resulting from electromigration are formed adjacent to one of the two electrodes leaving a portion of the ER fluid relatively clear of particles and hence leading to a reduction in the resistance against externally applied shear forces perpendicular to the electric field and a decrease in the modulus or the effective viscosity is measured—the negative ER effect [5]-[6].

Despite the relatively sparse reports on negative ER effects, recent experimental observations found that: (i) with a given constant shear rate or equivalently the Couette boundary driving velocity, the measured shear stress required to drive the Couette ER fluid flow is reduced (an effectively decreased viscosity) and (ii) at a given constant pressure gradient, the Poiseuille flow rate of the ER fluid can be increased for both flows by applying a uniform direct current (DC) electric field perpendicular to the direction of the flows [7]-[12]. The mechanism responsible for the apparent increased flow rate or

decreased effective viscosity was attributed to the spontaneous electrorotation of the dielectric micro-particles suspended within the carrier liquid, which is a mechanism different from the traditional electrophoresis or electro-migration explanation as mentioned in previous negative ER literature. This spontaneous particle rotation under the action of a DC electric field is often called "Quincke rotation" for von G. Quincke's systematic study done in 1896 [13]-[18].

The origin of Quincke rotation can be illustrated by considering a collection of insulating dielectric spherical particles with permittivity ε_2 and conductivity σ_2 suspended in a slightly conducting carrier liquid having a permittivity of ε_1 and a conductivity of σ_1. The material combination is chosen so that $\tau_2 > \tau_1$ where $\tau_1 = \varepsilon_1/\sigma_1$ and $\tau_2 = \varepsilon_2/\sigma_2$ are the relaxation time constants of the liquid and the particles, respectively. When a uniform DC electric field is applied across the suspension, charge relaxation occurs according to the Maxwell-Wagner (MW) polarization at the solid-liquid interfaces, and each of the suspended particles attains a final equilibrium dipole moment in the opposite direction to that of the applied DC field for the condition of $\tau_2 > \tau_1$, *i.e.*, liquid relaxes faster than particle. This, however, is an unstable equilibrium, and as the applied electric field reaches some critical value [17]-[18], namely,

$$E_c \equiv \left(1+\frac{\sigma_2}{2\sigma_1}\right)\sqrt{\frac{8\eta_0\sigma_1}{3\varepsilon_1\sigma_2(\tau_2-\tau_1)}}, \qquad (1)$$

where η_0 is the viscosity of the carrier liquid, the liquid viscous torque can no longer withstand any small perturbations on the particles whence giving rise to spontaneous, self-sustained particle rotation either clockwise or counter clockwise (with the rotation axis perpendicular to the planes defined by the electric field) due to the electrical torque arising from the misalignment of the particle dipole moment and the applied DC field.

When the particle-liquid suspension or ER fluid is driven by a boundary shear stress (Couette) or a pressure gradient (Poiseuille), the macroscopic flow vorticity gives the suspended micro-particles, instead of by random chance, preferable directions for rotation via viscous interactions once the external electric field larger than the critical field, E_c, is applied. It is this combined effect of microscopic electrorotation and macroscopic flow vorticity that gives rise to the observed negative ER phenomenon as described above [7]-[12].

Although models are given in current literature for analyzing the present negative ER phenomenon, most of them are focused on the dynamics of a single particle and the utilization of a two-phase effective continuum description [7]-[12]. Little has been done in developing a continuum mechanical model from a more classical, field theory based perspective in predicting the dynamical behavior of fluids consisting of micro-particles undergoing spontaneous electrorotation. To the best of the authors' knowledge, the ferrofluid spin-up flow is the most representative flow phenomenon arising from internal particle rotation in current rheology research [19]-[26].

In a ferrofluid spin-up flow, magnetic torque is introduced into the ferrofluid, which consists of colloidally stabilized magnetic nanoparticles, typically magnetite, suspended in a non-magnetizable fluid, through the misalignment of the particle's permanent magnetization and the applied rotating magnetic field. From a macroscopic point of view, the introduced magnetic torque manifests itself through the ensemble of the particle-liquid interactions as the anti-symmetric component of the continuum stress tensor while the average effect of the internal particle rotation is reflected in the macro, continuum fluid hydrodynamic spin velocity. In order to describe how particle rotation affects the continuum flow motion, an angular momentum conservation equation is added and coupled with the linear momentum equation so that, in general, the externally applied magnetic body couple, angular momentum conversion between linear and spin velocity fields, and the diffusive transport of angular momentum are incorporated into the description of the flow momentum balances [21], [27]-[29].

A fundamental issue in the current development of ferrofluid spin-up flow is whether the diffusive angular momentum transport or couple stress has a finite contribution in the angular momentum balances of the flow. The current consensus is that the couple stress contribution is vanishingly small, *i.e.*, zero spin viscosity or diffusive transport conditions, as discussed in Rosensweig [21], Chaves *et al.* [25]-[26], Schumacher *et al.* [30], and so on. In a most recent work by Feng *et al.* [31], scaling and numerical analyses were presented to show that in the limit of an effective continuum, the angular momentum equation is to be couple stress free and the value of the spin viscosity should be identically zero. However, spin-up velocity profiles measured by ultrasound velocimetry reported by He [22], Elborai [23], and Chaves *et al.* [25]-[26] were compared with the numerical simulations of the full spin-up flow governing equations and found that the experimental and numerical results would agree only if the spin viscosity assumes some finite value instead of being vanishingly small or identically zero.

Acknowledging the experimental and theoretical discrepancies in the value of spin viscosity and identifying the "mathematically analogous, physically parallel mechanisms" governing the respective electrorotation and ferrofluid spin-up

TABLE I
SUMMARY OF PHYSICAL ANALOGY BETWEEN THE ELECTROROTATION AND FERROFLUID SPIN-UP FLOWS

	Electrorotation (Quincke rotation) flow	Ferrofluid spin-up flow
Particles	Insulating dielectric (plastic) micro-particle	Magnetic nano particles
Origin of micro scale polarity	Maxwell-Wagner (MW) polarization	Permanent magnetic dipole
Macroscopic polarity variable	Polarization $\overline{P}$ (due to induced free surface charge)	Magnetization $\overline{M}$
Applied field	DC electric field $\overline{E}$ (combined with flow vorticity)	Rotating magnetic field $\overline{H}$
Body torque density (Nm^{-2})	$\overline{P}\times\overline{E}$	$\mu_0\overline{M}\times\overline{H}$

flows (as summarized in Table I), this work is therefore aimed at developing a classical continuum mechanical model that combines particle electrorotation and anti-symmetric stress theories for describing the electrorheological behavior of a particle-liquid mixture (termed ER fluid henceforward) subjected to a DC electric field strength higher than the Quincke rotation threshold in both Couette and Poiseuille flow geometries. Emphasis is especially placed on investigating the effects of a zero spin viscosity, $\eta' = 0$, on the angular momentum balances in the flow or ER response. In the next section, the governing equations describing the mass conservation, linear momentum conservation, angular momentum conservation, and polarization relaxation of the ER fluid flow will be given in their most general forms. The specific governing equations, analytical solutions, and the evaluated numerical results are then presented, compared, and discussed in Sections III and IV to respectively show how the pertinent physical parameters are correlated with the ER responses and fluid flow in two dimensional (2D) Couette and Poiseuille flows with internal particle electrorotation. A concluding section will be given at the end of this article to summarize the principle findings of the present article and the motivations for future research.

II. MATHEMATICAL FORMULATION

In order to quantitatively model and describe the present ER flow phenomenon, several physical principles involved are considered: (i) the continuity or mass conservation, (ii) the linear momentum balance, (iii) the angular momentum balance, and (iv) the polarization relaxation of the ER fluid flow. The governing equations are given in the following subsections to describe the above physical principles in proper mathematical forms.

A. The Fluid Mechanical Equations

The equations describing the ER fluid motion are the mass continuity equation for incompressible flow,

$$\nabla \cdot \bar{v} = 0, \tag{2}$$

the linear momentum equation,

$$\rho \frac{D\bar{v}}{Dt} = -\nabla p + \left(\bar{P}_t \cdot \nabla\right)\bar{E} + 2\zeta \nabla \times \bar{\omega} + \beta \nabla\left(\nabla \cdot \bar{v}\right) + \eta_e \nabla^2 \bar{v}, \tag{3}$$

and the angular momentum equation,

$$I \frac{D\bar{\omega}}{Dt} = \bar{P}_t \times \bar{E} + 2\zeta\left(\nabla \times \bar{v} - 2\bar{\omega}\right) + \beta' \nabla\left(\nabla \cdot \bar{\omega}\right) + \eta' \nabla^2 \bar{\omega}, \tag{4}$$

where $\bar{v}$ is the linear flow velocity, ρ is the ER fluid density, p is the pressure in the flow field, $\bar{P}_t$ is the fluid total polarization, $\bar{E}$ is the electric field, $\bar{\omega}$ is the flow spin velocity, I is the average moment of inertia per unit volume, η' is the spin viscosity, ζ is the vortex viscosity which is related to the carrier liquid viscosity, η_0, and particle solid fraction, ϕ, through $\zeta \approx 1.5\phi\eta_0$ for dilute suspensions with $\phi \ll 1$, $\beta = \lambda + \eta - \zeta$ is the sum of the second coefficient of viscosity, λ, the zero field ER fluid viscosity, $\eta \approx \eta_0(1 + 2.5\phi)$, and the negative of the vortex viscosity, $\eta_e = \eta + \zeta$ is the sum of the zero field ER fluid viscosity and the vortex viscosity, $\beta' = \eta' + \lambda'$ is the sum of the spin viscosity and the second coefficient of spin viscosity, λ' [21], [28], [32], and D/Dt is the material derivative given by

$$\frac{D}{Dt} = \frac{\partial}{\partial t} + \left(\bar{v} \cdot \nabla\right). \tag{5}$$

Note that (3) generally follows the form of the well known Navier-Stokes equation. However, by introducing particle rotation to the fluid flow, additional terms are included in (3) to account for the Kelvin body force density, $\left(\bar{P}_t \cdot \nabla\right)\bar{E}$, and the anti-symmetric force density, $2\zeta \nabla \times \bar{\omega}$, contributions in the linear momentum balances of the fluid flow. Moreover, (4) characterizes the ER fluid rotation velocity, or spin velocity, so that the torque and angular momentum balances resulting from the electrical torque input and fluid motion can be described and related to other variables pertinent to this problem. In (4), the left hand side represents the angular momentum of a continuum ER fluid particle; the first term on the right hand side (RHS) represents the electrical torque introduced to the flow field via the rotating micro-particles under the action of the external DC field; the second term on the RHS represents the angular momentum transformation or conversion between the vorticity and the spin velocity fields; the third term on the RHS represents the gradient of the divergence of the spin velocity and is analogous to the "gradient of the divergence of the velocity" term in (3) that measures the bulk compression effects in the fluid flow; and finally, the fourth term on the RHS represents the diffusive transport of angular momentum within the flow field [21].

B. The Electro-quasi-static (EQS) and the Polarization Relaxation Equations

The electric field in the ER flow field is described by the electro-quasi-static (EQS) Maxwell equations [16], [33]

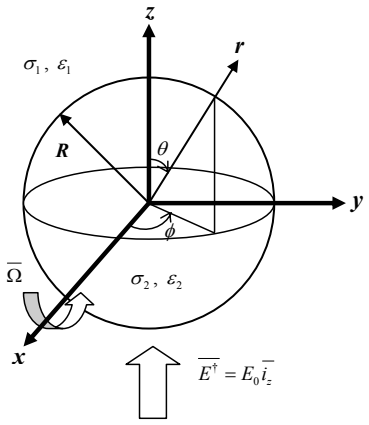

FIG. 1. The schematic diagram for the problem of solving the EQS field around a spherical particle of radius R (with conductivity of σ_2 and permittivity of ε_2) suspended in a liquid medium (with σ_1, ε_1) rotating at constant angular velocity $\bar{\Omega} = \Omega \bar{i}_x$ subjected to a uniform DC electric field, $\bar{E}^{\uparrow} = E_0 \bar{i}_z$.

namely,

$$\nabla \times \overline{E} \approx 0 \text{, and} \tag{6}$$

$$\nabla \cdot \overline{D} = \rho_f \approx 0 \text{,} \tag{7}$$

where $\overline{D}$ is the displacement field and ρ_f is the free space charge density. Here, we have assumed that on the macroscopic continuum level, the free space charge is zero. To complete the description of the electrical subsystem, we need a continuum phenomenological polarization relaxation equation that accounts for the non-equilibrium effects of both the linear and angular motions on the ER fluid polarization. Since the torque input on the micro scale is related to the surface charge around the surface of the micro-particles, we shall focus on how non-equilibrium motion, *i.e.*, micro-particle rotation, $\overline{\Omega}$, continuum fluid spin velocity, $\overline{\omega}$, and continuum fluid velocity, $\overline{v}$, affects the retarding polarization (the part of polarization directly related to the surface charges) instead of the total polarization of the ER fluid. We start the construction of the polarization relaxation equation and its equilibrium polarization from the micro scale.

The problem of the EQS field around a spherical particle suspended in a liquid medium rotating at a constant speed, $\overline{\Omega} = \Omega \overline{i_x}$, subjected to a uniform electric field, $\overline{E^\dagger} = E_z^\dagger \overline{i_z} = E_0 \overline{i_z}$ ($\dagger$ denotes microscopic field quantities), as shown in Fig. 1 has been solved by Cebers [34]. Here, we only summarize the solutions to the electric potential and the dipole moment of the particle for $r > R$, where R is the radius of the micro-particle. The outer electric potential ($r > R$) is given in spherical coordinates as

$$\begin{aligned} \Phi^\dagger(r,\theta,\phi) &= -rE_0\cos\theta + \frac{\overline{p_t^\dagger}\cdot\overline{i_r}}{4\pi\varepsilon_1 r^2} \\ &= -rE_0\cos\theta + \frac{4\pi\varepsilon_1}{4\pi\varepsilon_1 r^2}\left(a_3\cos\theta + a_6\sin\phi\sin\theta\right) \end{aligned}, \tag{8}$$

where

$$a_3 = E_0 R^3 \left[\frac{\varepsilon_2 - \varepsilon_1}{2\varepsilon_1 + \varepsilon_2} + \frac{\left(\frac{\sigma_2 - \sigma_1}{2\sigma_1 + \sigma_2} - \frac{\varepsilon_2 - \varepsilon_1}{2\varepsilon_1 + \varepsilon_2} \right)}{1 + \tau_{MW}^2 \Omega^2} \right], \tag{9}$$

$$a_6 = -E_0 R^3 \frac{\left(\frac{\sigma_2 - \sigma_1}{2\sigma_1 + \sigma_2} - \frac{\varepsilon_2 - \varepsilon_1}{2\varepsilon_1 + \varepsilon_2} \right) \tau_{MW} \Omega}{1 + \tau_{MW}^2 \Omega^2}, \tag{10}$$

$$\overline{p_t^\dagger} = p_x^\dagger \overline{i_x} + p_y^\dagger \overline{i_y} + p_z^\dagger \overline{i_z} \text{,} \tag{11}$$

$$\overline{i_r} = \sin\theta\cos\phi\,\overline{i_x} + \sin\theta\sin\phi\,\overline{i_y} + \cos\theta\,\overline{i_z} \text{,} \tag{12}$$

and

$$\tau_{MW} \equiv \frac{2\varepsilon_1 + \varepsilon_2}{2\sigma_1 + \sigma_2} \text{,} \tag{13}$$

is the MW relaxation time. Using (8)-(12), we can find the total dipole moment of the rotating particle, $\overline{p_t^\dagger}$, as $p_x^\dagger = 0$, $p_y^\dagger = 4\pi\varepsilon_1 a_6$, and $p_z^\dagger = 4\pi\varepsilon_1 a_3$, and the retarding part of the dipole moment is then found as

$$\overline{p^\dagger} = 4\pi\varepsilon_1 a_6 \overline{i_y} + 4\pi\varepsilon_1 \left(a_3 - E_0 R^3 \frac{\varepsilon_2 - \varepsilon_1}{2\varepsilon_1 + \varepsilon_2} \right) \overline{i_z} \text{.} \tag{14}$$

The surface charge around the spherical particle with half of the hemisphere having positive charge and the other half having negative charge is directly related to the retarding dipole moment (14) [34]. By applying a torque balance between the electric torque, $\overline{p_t^\dagger} \times \overline{E^\dagger} = \overline{p^\dagger} \times \overline{E^\dagger} = 4\pi\varepsilon_1 a_6 E_0 \overline{i_x}$, and the viscous torque, $-8\pi\eta_0 \Omega R^3 \overline{i_x}$, on the particle in steady state, we can find the critical electric field for Quincke rotation as given in (1) and the rotation velocity of the micro-particle being [18]

$$\Omega = \pm \frac{1}{\tau_{MW}} \sqrt{\left(\frac{E_0}{E_c} \right)^2 - 1} \text{,} \tag{15}$$

where the + and - signs denote counter clockwise and clockwise rotation with the coordinate system defined in Fig. 1. In (15), we have assumed that the particle rotation is only in the *x*-direction; this is because we will only be considering 2D flow geometries in the following discussions. Note however that for the most general cases, the particle rotation axis is perpendicular to the planes defined by the electric field, which has a three dimensional feature.

We next consider a dilute particle suspension with a solid volume fraction of ϕ and a particle number density of n subjected to the DC electric field. The solid volume fraction and the particle number density are related through

$$\phi = n\left(\frac{\pi d^3}{6} \right) \sim O\left(nR^3 \right) \text{,} \tag{16}$$

where $d = 2R$ is the diameter of the micro-particle. Assuming that the mutual electrical interactions between the suspended micro-particles can be neglected (*i.e.*, dilute suspension), the macroscopic *retarding* polarization of the ER fluid at equilibrium, $\overline{P_{eq}}$, can be obtained by applying Maxwell's effective medium theory [18] or spatial averaging based on a unit cell of the suspension [34]. The final results can be easily obtained by multiplying (14) with the particle number density, n, *i.e.*, $\overline{P_{eq}} = P_{eq}^y \overline{i_y} + P_{eq}^z \overline{i_z}$ with

$$\begin{bmatrix} P_{eq}^y \\ P_{eq}^z \end{bmatrix} = 4\pi\varepsilon_1 n R^3 \begin{bmatrix} -\frac{\tau_{MW}\Omega\left(\frac{\sigma_2 - \sigma_1}{2\sigma_1 + \sigma_2} - \frac{\varepsilon_2 - \varepsilon_1}{2\varepsilon_1 + \varepsilon_2} \right)}{1 + \tau_{MW}^2 \Omega^2} \\ \frac{\left(\frac{\sigma_2 - \sigma_1}{2\sigma_1 + \sigma_2} - \frac{\varepsilon_2 - \varepsilon_1}{2\varepsilon_1 + \varepsilon_2} \right)}{1 + \tau_{MW}^2 \Omega^2} \end{bmatrix} E_0 \text{.} \tag{17}$$

Equation (17) represents the macroscopic retarding polarization of a static, motionless ER fluid, namely, $\overline{\omega} = 0$ and $\overline{v} = 0$. Yet, this does not mean that at macroscopic equilibrium, the micro-particles are not rotating on the microscopic level, *i.e.*. $\overline{\Omega} \neq 0$, when the applied electric field is larger than the critical electric field given in (1), that is, $E_0 \geq E_c$. This idea is similar to the dynamic effective medium model shown in the work of Xiao *et al.* [35]. As for the cases of $E_0 < E_c$, Ω is set to zero in (17) since an applied field less than the critical field will give imaginary values of Ω and the real root can only be zero. Combining (15) and (17) and extending the physical arguments

of the phenomenological magnetization relaxation equation proposed by Shliomis [21], [36]-[37] to the case of the retarding polarization, we arrive at the following retarding polarization relaxation equation,

$$\frac{D\overline{P}}{Dt}=\left(\overline{\omega}\times\overline{P}\right)-\frac{1}{\tau_{MW}}\left(\overline{P}-\overline{P_{eq}}\right), \tag{18}$$

where $\overline{P}$ is the retarding polarization.

Equations (15)-(18) account for the non-equilibrium effects of micro-particle rotation velocity, $\overline{\Omega}$, fluid spin velocity, $\overline{\omega}$, and fluid translation velocity, $\overline{v}$, on the retarding polarization, or more specifically, charge relaxation. Rigorously speaking, the particle rotation speed in (15) should be corrected both kinematically and dynamically for the differences in rotation speeds arising from different frames of reference. The particle rotation speed, $\overline{\Omega}$, that enters (17) and (18) should be the speed observed in the reference frame of the ER fluid spin velocity, $\overline{\omega}$. Yet, as a first approach, we use (15) to be the particle rotation velocity that enters (17) and (18). Practically speaking, inclusion of the frame correction on $\overline{\Omega}$ will cause numerical difficulties in the evaluation of the spin velocity solutions, $\overline{\omega}$. As will be seen in the following, the governing equations will be reduced into third order algebraic equations for both Couette and Poiseuille flows. Therefore, there will in general be two sets of three roots for $\overline{\omega}$ with the roots changing from real to imaginary valued or vice versa depending on the parametric regimes of interests for both flows, respectively. While only the real valued solutions are valid in the solution process, a frame of reference correction to the particle rotation speed $\overline{\Omega}$ used in (17) and (18) will cause the real valued solution to jump among all three roots of $\overline{\omega}$ instead of one or two uniformly valid roots through out the evaluation domains. If all three roots contribute to the real valued solution of $\overline{\omega}$, we will need to exactly pin point the parametric regimes in which the solution changes from real to imaginary and vice versa for each root, causing the solution process to be much more involved and generally does not improve the solution to a greater deal of accuracy as compared to the experimental results. The solutions without the reference frame correction presented herein slightly under predicts the reduction in the effective viscosity at high shear rates and electric field strengths as compared to those done with a first attempt of reference frame correction for Couette flows.

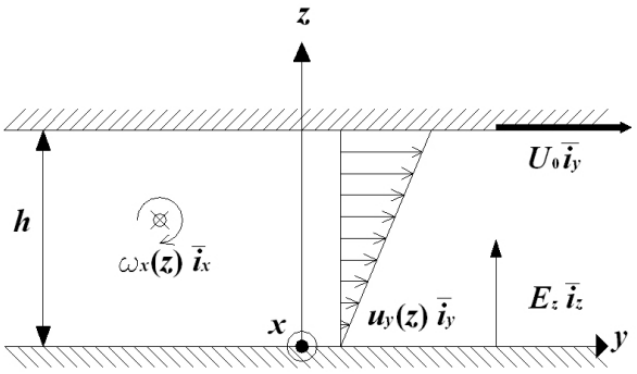

FIG. 2. The schematic diagram illustrating the geometry, dimensions, and physical parameters for Couette flow with internal particle electrorotation.

III. Couette Flow with Internal Particle Electrorotation

A. The Governing Equations Specific to the Couette Flow Geometry

Consider the Couette flow geometry shown in the schematic diagram of Fig. 2. The lower plate of the parallel plate system is fixed at zero velocity while the upper plate is applied with a constant velocity, U_0, in the positive *y*-direction. We assume that the flow is steady ($\partial/\partial t=0$), incompressible, fully developed ($\partial/\partial y=0$), and two-dimensional ($\partial/\partial x=0$) in Cartesian coordinates. Under these assumptions, the continuity equation, (2), is readily reduced to $du_z/dz=0$ and subsequently to $u_z=0$ since the *z*-velocity component, u_z, has to satisfy the no-slip and non-penetrating (impermeable walls) boundary conditions at $z=0$ and h with h being the height of the 2D channel. Moreover, by using the EQS Faraday's equation, (6), with the condition of fully developed flow, we find $dE_y/dz=0$ such that E_y is just a constant throughout the 2D channel. Noting that the boundaries at $z=0$ and h are perfectly conducting electrodes, and that the tangential component of the electric field is continuous across the boundaries, the constant E_y is simply zero. Therefore, the applied DC electric field is to be in the *z*-direction only. The fringing effects at the ends of the channel are to be neglected.

The governing equations are further simplified by considering a zero spin viscosity, *i.e.*, $\eta'=0$, in the angular momentum equation, (4). Given the above assumptions combined with the continuity and zero spin viscosity conditions, (3), (4), and (18), are then simplified into the following:

$$-\tau_{MW}\omega_x P_z-\left(P_y-P_{eq}^y\right)=0, \tag{19a}$$

$$\tau_{MW}\omega_x P_y-\left(P_z-P_{eq}^z\right)=0, \tag{19b}$$

$$2\zeta\frac{d\omega_x}{dz}+\eta_e\frac{d^2u_y}{dz^2}=0, \tag{20}$$

and

$$P_yE_z+2\zeta\left(-\frac{du_y}{dz}-2\omega_x\right)=0, \tag{21}$$

where u_y is the *y*-velocity component, ω_x is the *x*-spin velocity component, E_z is the *z*-component of the applied DC electric field, and P_y and P_z are the retarding polarization components in the *y*- and *z*- directions, respectively. Note that we have substituted the total polarization, P_{ty}, with the retarding polarization, P_y, in (21). This is because the DC electric field is applied in the *z*-direction only with $E_y=0$. Thus the total polarization in the *y*-direction comes from the dipole moment tilt of the rotating micro-particles in the micro scale, which, on the macroscopic level, is generally the *y*-component of the retarding polarization [34]. Finally, the *z*-linear momentum equation reduces to an equation which relates only the pressure gradient to the dielectric body force, and thus can be treated separately from the other equations.

Substituting (17) into (19), we can solve for the *y*- and *z*-components of the retarding polarization as

$$P_y = n\frac{\alpha_y - \tau_{MW}\omega_x\alpha_z}{1+\tau_{MW}^2\omega_x^2}E_0\,, \tag{22a}$$

$$P_z = n\frac{\alpha_z + \tau_{MW}\omega_x\alpha_y}{1+\tau_{MW}^2\omega_x^2}E_0\,, \tag{22b}$$

where

$$\begin{bmatrix}\alpha_y\\ \alpha_z\end{bmatrix} = 4\pi\varepsilon_1 R^3 \begin{bmatrix} -\dfrac{\tau_{MW}\Omega\left(\dfrac{\sigma_2-\sigma_1}{2\sigma_1+\sigma_2}-\dfrac{\varepsilon_2-\varepsilon_1}{2\varepsilon_1+\varepsilon_2}\right)}{1+\tau_{MW}^2\Omega^2} \\ \dfrac{\left(\dfrac{\sigma_2-\sigma_1}{2\sigma_1+\sigma_2}-\dfrac{\varepsilon_2-\varepsilon_1}{2\varepsilon_1+\varepsilon_2}\right)}{1+\tau_{MW}^2\Omega^2} \end{bmatrix}, \tag{23}$$

with Ω given in (15). We substitute (22a) into (21) and recognizing that the macroscopic (averaged) field and is related to the microscopic electric field through

$$\overline{E} = \overline{E^\dagger} - \frac{3\phi}{R^3}\left(a_6\overline{i_y} + a_3\overline{i_z}\right) = E_0\overline{i_z} - \frac{3\phi}{R^3}\left(a_6\overline{i_y} + a_3\overline{i_z}\right), \tag{24}$$

as derived by Cebers [34], we approximate to the first order of magnitude of the volume fraction, ϕ ($nR^3 \sim nd^3 \sim O(\phi)$ as in (16)), $\overline{E} = E_z\overline{i_z} \approx \overline{E^\dagger} = E_0\overline{i_z}$ for dilute suspensions (using this approximation, we decouple the electrical field equations, (6)-(7), from the mechanical field equations, (2)-(4)). Hence the governing equations specific to the Couette flow geometry with internal particle electrorotation is obtained as

$$2\zeta\frac{d\omega_x}{dz} + \eta_e\frac{d^2u_y}{dz^2} = 0\,, \tag{20}$$

and

$$\frac{\alpha^* - \tau_{MW}\omega_x}{1+\tau_{MW}^2\omega_x^2}n\alpha_z E_0^2 + 2\zeta\left(-\frac{du_y}{dz} - 2\omega_x\right) = 0\,. \tag{25}$$

with $\alpha^* = \alpha_y/\alpha_z$. The boundary conditions for the velocity field, $\overline{v} = u_y\,\overline{i_y}$, is the general no-slip boundary condition, *i.e.*, $\overline{v} = 0$ at $z = 0$ and $\overline{v} = U_0\,\overline{i_y}$ at $z = h$. On the other hand, the angular momentum equation, (25), eventually reduces to an algebraic equation for zero spin viscosity conditions as will be discussed shortly in Section III.B; hence, there are no additional constraints to be applied at the boundaries for the Couette spin velocity field. This "free-to-spin" condition on ω_x for $\eta' = 0$ is likely an analogous case to the Euler equation for inviscid fluid flow—the linear flow velocity is allowed to slip at the solid-fluid boundaries when the fluid viscosity goes to zero.

B. Solutions to the Spin Velocity and the Effective Viscosity

Integrating (20) with respect to *z*, we have

$$2\zeta\omega_x + \eta_e\frac{du_y}{dz} = C_c\,, \tag{26}$$

where C_c is a constant. Substituting (26) into (25), we find that the spin velocity, ω_x, does not depend on the spatial coordinate, *z*, and therefore (20) reduces to the original governing equation for simple Couette flow, *i.e.*,

$$\frac{d^2u_y}{dz^2} = 0\,, \tag{27}$$

and the solution to (27) is

$$u_y(z) = \frac{U_0}{h}z\,. \tag{28}$$

Inserting (28) into (25) and using the following non-dimensionalization scheme, namely,

$$\omega^* = \tau_{MW}\omega_x\,,\ \gamma^* = \tau_{MW}\frac{U_0}{h}\text{, and } M^* = \frac{2\zeta}{n\alpha_z E_0^2\tau_{MW}}\,, \tag{29}$$

the non-dimensional angular momentum equation is obtained as

$$\omega^{*3} + \frac{\gamma^*}{2}\omega^{*2} + \left(1+\frac{1}{2M^*}\right)\omega^* + \left(\frac{\gamma^*}{2} - \frac{\alpha^*}{2M^*}\right) = 0\,. \tag{30}$$

Equation (30) can be solved to obtain analytical expressions by symbolic calculation packages (Mathematica, Wolfram Research, Inc.) and the three roots of (30) are expressed as functions of γ^* and M^*. Nevertheless, it should be pointed out that not all the three roots to ω^* are likely to be physically meaningful and interpretable for the flow phenomena of interest presented herein. In order to find the most physically meaningful and interpretable solution or combination of solutions from the three (at most) possible solutions to the current problem, the following considerations and conditions are applied to the flow field: (i) the ER fluid is "free-to-spin" at the solid-ER fluid boundaries since the governing physics reduce from a boundary value problem to an algebraic problem in zero spin viscosity flows and (ii) the micro- particle angular velocity, $\overline{\Omega}$, [7]-[12] and subsequently the macroscopic fluid spin velocity, $\overline{\omega}$, rotate in the same direction as that of the macro scale flow vorticity so that the particle and ER fluid rotation is always stable. We have shown that the spin velocity is a constant throughout the channel when $\eta' = 0$ in the Couette geometry. Hence, ω^* assumes some finite value at the solid-ER fluid boundaries, which is readily self-consistent with the "free-to-spin" condition. To satisfy condition (ii), we need to single out the solution to ω^* (or ω_x) that has the same negative sign (or clockwise rotation) as the macroscale Couette flow vorticity, namely, $\nabla\times\overline{v} = -\left(du_y/dz\right)\overline{i_x} = -\left(U_0/h\right)\overline{i_x}$, with the coordinate system defined in Fig. 2. We also pick the negative valued solution for the particle rotation speed, Ω, given in (15) and substitute Ω into (17) and (23) to solve (30). For the parametric regimes of our interests, we identify the stable solution to the spin velocity as (solved by Mathematica under "Solve" command)

$$\omega_{C2}^* = -\frac{\gamma^*}{6} - \varphi_{C1}\left(1+i\sqrt{3}\right)\left[6\sqrt[3]{4}M^*\left(\varphi_{C2}+\sqrt{4\varphi_{C1}^3+\varphi_{C2}^2}\right)^{1/3}\right]^{-1} + \frac{1}{12\sqrt[3]{2}M^*}\left[\left(1-i\sqrt{3}\right)\left(\varphi_{C2}+\sqrt{4\varphi_{C1}^3+\varphi_{C2}^2}\right)^{1/3}\right] \tag{31}$$

for $E_0 \geq E_c$, and

$$\omega_{C1}^{*}=-\frac{\gamma^{*}}{6}+\varphi_{C1}\left[3\sqrt[3]{4}M^{*}\left(\varphi_{C2}+\sqrt{4\varphi_{C1}^{3}+\varphi_{C2}^{2}}\right)^{1/3}\right]^{-1}-\frac{1}{6\sqrt[3]{2}M^{*}}\left(\varphi_{C2}+\sqrt{4\varphi_{C1}^{3}+\varphi_{C2}^{2}}\right)^{1/3},\quad(32)$$

for $E_0 < E_c$, where

$$\varphi_{C1}=6M^{*}+12M^{*2}-M^{*2}\gamma^{*2},\quad(33)$$

and

$$\varphi_{C2}=-18M^{*2}\gamma^{*}+72M^{*3}\gamma^{*}+2M^{*3}\gamma^{*3}-108M^{*2}\alpha^{*}.\quad(34)$$

Notice that in evaluating solution in the regime of $E_0 < E_c$, the micro-particle rotation speed, Ω, is set to zero in (17) and (23) since for $E_0 < E_c$, (15) will give an imaginary value to the particle rotation speed.

The effective viscosity of Couette flows with particle electrorotation, η_{eff}, is derived by recognizing the relationship between the wall shear stress, τ_s, and the average shear rate (or the velocity of the upper plate, U_0, divided by the channel height, h) when the shear stress is held constant for a given flow or experimental condition, *i.e.*,

$$\tau_s=\eta_{eff}\frac{U_0}{h}=\eta_{eff}\frac{\gamma^{*}}{\tau_{MW}}=\bar{i}_z\cdot[\![\bar{\bar{T}}]\!]\cdot\bar{i}_y,\quad(35a)$$

in which $[\![\ ]\!]$ denotes the shear stress differences across the solid-liquid interface and $\bar{\bar{T}}=\bar{\bar{T}}_s+\bar{\bar{T}}_a$ is the total stress tensor with the symmetric part being

$$\bar{\bar{T}}_s=-p\bar{\bar{I}}+\eta\left[\nabla\bar{v}+\left(\nabla\bar{v}\right)^{t}\right],\quad(35b)$$

and the antisymmetric part being

$$\bar{\bar{T}}_a=\zeta\bar{\bar{\varepsilon}}\cdot\left(\nabla\times\bar{v}-2\bar{\omega}\right),\quad(35c)$$

[21]. By expanding the total stress tensor into matrix form and substituting the velocity field, (28), and the spin velocity field, (31) or (32), into (35), the effective viscosity can be obtained as

$$\eta_{eff}=\eta_e+2\zeta\frac{\omega^{*}}{\gamma^{*}},\quad(36a)$$

or in dimensionless terms,

$$\eta^{*}\equiv\frac{\eta_{eff}}{\eta}=\frac{\eta_e}{\eta}+\frac{2\zeta}{\eta}\frac{\omega_{Ci}^{*}}{\gamma^{*}},\quad(36b)$$

where $\omega_{Ci}^{*}=\omega_{C1}^{*}$ or ω_{C2}^{*} depending on the electric field strength and $\eta\approx\eta_0(1+2.5\phi)$ is the zero field ER fluid (particle-liquid mixture) viscosity as defined in Section II.A. The shear stress differences in (35a) are all evaluated at $z=0$ in this article.

C. Results and Discussions

After obtaining the velocity and spin velocity fields as well as the effective viscosity, we now further present the numerical evaluations of the analytical expressions given in (31), (32), and (36). The system parameters, physical constants, and material properties used in our evaluations follow those given in [7]-[12] so as to facilitate a more effective comparison between the current continuum model and the two-phase effective continuum formulations found in the literature. These data are summarized in Table II.

TABLE II
SYSTEM PARAMTERS, PHYSICAL CONSTANTS, AND MATERIAL PROPERTIES USED IN THE NUMERICAL CALCULATIONS [7]-[12]

Item	Description	Value	Units
d	Micro-particle diameter	8.00×10^{-5}	m
E_c	Critical electric field strength	1.30×10^{6}	$V\cdot m^{-1}$
h	Channel height	1.00×10^{-3}	m
n	Particle number density	3.73×10^{11}	m^{-3}
ε_1	Permittivity of carrier liquid	3.27×10^{-11}	$C^2N^{-1}m^{-2}$
ε_2	Permittivity of particles	2.30×10^{-11}	$C^2N^{-1}m^{-2}$
ϕ	Solid volume fraction of the particles	1.00×10^{-1}	--
η_0	Carrier liquid viscosity (no particles)	1.20×10^{-2}	$Pa\cdot s$
η'	Spin viscosity	0	$N\cdot s$
η	Zero field fluid viscosity (w/ particles)	1.53×10^{-2}	$Pa\cdot s$
η_e	$\eta_e=\eta+\zeta$	1.76×10^{-2}	$Pa\cdot s$
σ_1	Conductivity of the carrier liquid	4.00×10^{-8}	$S\cdot m^{-1}$
σ_2	Conductivity of the particles	1.00×10^{-14}	$S\cdot m^{-1}$
τ_{MW}	Maxwell-Wagner relaxation time	1.11×10^{-3}	s
ζ	Vortex viscosity	1.80×10^{-3}	$Pa\cdot s$

Shown in Fig. 3 is the Couette spin velocity, $\omega^{*}=\tau_{MW}\omega_x$, given by (31), *i.e.*, $\omega^{*}=\omega_{C2}^{*}$, for $E_0\geq E_c$ (with the particle rotation speed Ω chosen to be negative in (15), (17), and (23)) and by (32), *i.e.*, $\omega^{*}=\omega_{C1}^{*}$, for $E_0 < E_c$ (with Ω set to zero in (17), (23)) plotted with respect to the average shear rate, $\gamma^{*}=\tau_{MW}U_0/h$, evaluated at $E^{*}=E_0/E_c=0$, 0.4, 0.8, 1.0, 2.0, and 3.0 where $E_c=1.3\times10^{6}$ (Vm^{-1}) is the critical electric field for the onset of particle Quincke rotation evaluated by (1) with the material properties given in Table II. The negative values of ω^{*} given in the figure indicate that the ER fluid rotates or spins in the same clockwise direction (*i.e.*, -*x*-direction of the coordinate system shown in Fig. 2) as that of the macroscale Couette flow vorticity so that the stable rotation condition can be satisfied. Moreover, it is learned from Fig. 3 that the magnitude of the spin velocity within the flow field increases as the applied electric field strength is increased with γ^{*} kept constant. On the other hand, the fluid spin magnitude also increases as the average shear rate, γ^{*}, or the applied velocity of the upper boundary, U_0, increases while the field strength is kept constant. As the applied electric field, E_0 or E^{*}, is reduced to zero, the ER fluid spin velocity reduces back to the angular velocity of a continuum fluid parcel, *i.e.*, $\omega_0^{*}=-\gamma^{*}/2$, half of the Couette flow vorticity which can be readily deduced from (30) by letting $M^{*}\to\infty$ or $E_0\to0$. This solution is noted by the gray line with $E^{*}=0$ in Fig. 3.

Notice that for a given field strength and shear rate, the spin velocity, ω^{*} or ω_x, is a constant throughout the channel and, thus, does not depend on the spatial *z*-coordinate as already discussed in Section III.B for the Couette geometry. With the spin velocity being a constant in (20), the velocity field of Couette flow with internal particle electrorotation is found to be the same as that of Couette flow *without* particle electrorotation—a result consistent with those given in Shliomis [38] and Rosensweig [21]. Thus, the velocity field of Couette flow with particle electrorotation is not further

presented herein since plots of the linear profile given by (28) can be easily found in standard fluid mechanics text books.

Figure 4 shows the effective viscosity, $\eta^* = \eta_{eff}/\eta$, of Couette flow with internal particle electrorotation as given in (36). The effective viscosity is plotted with respect to the average shear rate, γ^*, with the electric field strength being evaluated at $E^* = 0$, 0.4, 0.8, 1.0, 2.0, and 3.0. It is readily seen that the effective viscosity decreases as the applied DC electric field strength increases. However, as the magnitude of the shear rate increases, the amount of reduction in the effective viscosity decreases regardless of the applied electric field strength. We further point out that since the effective viscosity is normalized and non-dimensionalized by the ER fluid viscosity when no electric field is applied, the value of η^* should approach to one as the applied electric field goes to zero, which is a result easily found by substituting $\omega_0^* = -\gamma^*/2$ into (36). The zero electric field result is indicated by the gray line in Fig. 4. It can be seen from the figure that the predicted effective viscosities η^* approach to one when the shear rate, γ^*, goes large or the applied electric field goes to zero.

From Fig. 4, we find that zero or negative viscosities are attainable when the applied DC electric field strength is strong enough. By using the terms "zero or negative viscosities," we do not mean that the true fluid viscosity is zero or negative, but that the effective or apparent viscosity mathematically sums up to be zero or a negative value through performing the force balance described by (35) and (36) when the boundary shear stress, τ_s, is maintained a constant. In experimental terms, as the applied electric field strength goes large, the "pumping" or "conveyer belt" effect of the micro-particles undergoing electrorotation on the fluid continuum becomes so significant that the ER fluid spin or rotation itself, instead of some externally applied force or torque, provides the shear stress required to move the upper plate of the Couette geometry. Therefore, we observe a finite shear rate, γ^*, or plate velocity, U_0, while the readings on the rheometer indicate a zero torque applied to the fluid. For the negative effective viscosity conditions, the electrorotation pumping is even more significant that the rheometer eventually has to "pull back" the upper plate to observe a certain finite value of shear rate or plate velocity. Further discussions can be found in Lobry and Lemaire [7] for the experimental considerations and in Zahn and Greer [39] and Zahn and Pioch [40]-[41] for explanations of positive, zero, and negative viscosity measurements.

The effective viscosity solution given in the present continuum model can be compared with the results found in Pannacci *et al.* [11] and Lemaire *et al.* [12] by using the same $\sigma_1 = 1.5\times10^{-8}$ (Sm^{-1}) for the carrier liquid conductivity and other material parameters given in the two references for the numerical calculations. We find that the continuum model predicted effective viscosity varies in a similar trend with respect to γ^* or E^* as compared with Fig. 2 in Pannacci *et al.* and Figs. 7(a) and 7(b) in Lemaire *et al.*. Unlike the model based on single particle dynamics in the two references which over estimates the reduction in effective viscosity, the present continuum model under estimates the reduction in η^* at high shear rates and electric field strengths, but falls closer to the experimental data shown in their work at relatively moderate shear rates and field strengths.

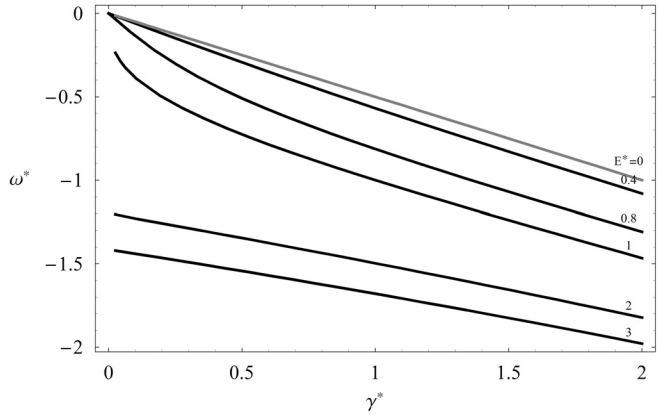

FIG. 3. The Couette spin velocity, ω^*, plotted with respect to the average shear rate, γ^*, evaluated at $E^* = 0$, 0.4, 0.8, 1.0, 2.0, and 3.0. For $E^* \geq 1.0$, the spin velocity given by (31), *i.e.*, $\omega^* = \omega_{C2}^*$, and a negative valued Ω from (15) is used in the evaluation, whereas $\omega^* = \omega_{C1}^*$ given by (32) is employed for cases of $E^* < 1.0$ with the micro-particle rotation speeds be set to zero in (17) and (23). The gray line denotes the zero electric field spin velocity, namely, half of the ER fluid vorticity.

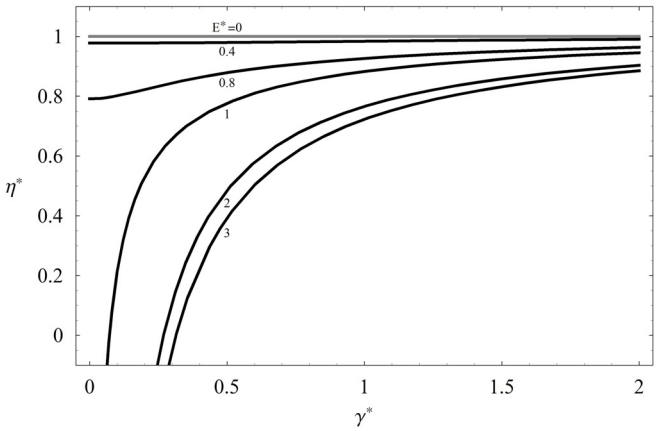

FIG. 4. The effective viscosity, η^*, found for Couette flow plotted with respect to the average shear rate, γ^*, evaluated at $E^* = 0$, 0.4, 0.8, 1.0, 2.0, and 3.0. For $E^* \geq 1.0$, the spin velocity given by (31), *i.e.*, $\omega^* = \omega_{C2}^*$ (with $\Omega < 0$ from (15) used in (17) and (23)), is used in the evaluation of (36), whereas $\omega^* = \omega_{C1}^*$ given by (32) is employed in (36) for cases of $E^* < 1.0$ with the micro-particle rotation speeds be set to zero in (17) and (23). The gray line denotes the zero electric field value of the effective viscosity, which is given by η in Table II.

IV. Poiseuille Flow with Internal Particle Electrorotation

A. The Governing Equations Specific to the Poiseuille Flow Geometry

Figure 5 shows the schematic diagram of a parallel plate Poiseuille flow. Instead of an upper plate moving at a constant velocity U_0, the upper and lower plates are now both fixed at zero velocity, and a pressure gradient, $\Gamma \equiv -\partial p/\partial y$, is applied in the positive *y*-direction, *i.e.*, $\Gamma > 0$, through the channel to drive

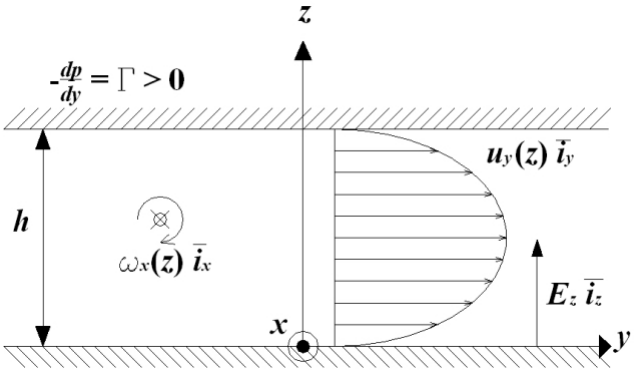

FIG. 5. The schematic diagram illustrating the geometry, dimensions, and physical parameters for Poiseuille flow with internal particle electrorotation.

the fluid flow. Based on the similar geometries given for both Couette and Poiseuille cases, we again assume that the flow is steady, incompressible, two-dimensional, and fully developed so that the *z*-velocity component, u_z, is identically zero and that the applied pressure gradient, Γ, is at most a constant for a fully developed flow. The applied DC electric field is further approximated to be only in the *z*-direction with $E_z = E_0$ and E_0 being a constant across the channel height, h.

For zero spin viscosity conditions, (3), (4), and (18) then reduce to (19), (21), and

$$\Gamma + 2\zeta \frac{d\omega_x}{dz} + \eta_e \frac{d^2 u_y}{dz^2} = 0 . \tag{37}$$

After substituting (17) into (19) and solving (19a) and (19b), we again arrive at (22) and (23). Using (22a) in (21), we obtain the following set of governing equations for Poiseuille flow with internal particle electrorotation, that is,

$$\Gamma + 2\zeta \frac{d\omega_x}{dz} + \eta_e \frac{d^2 u_y}{dz^2} = 0 . \tag{37}$$

and

$$\frac{\alpha^* - \tau_{MW}\omega_x}{1 + \tau_{MW}^2 \omega_x^2} n\alpha_z E_0^2 + 2\zeta \left(-\frac{du_y}{dz} - 2\omega_x \right) = 0 . \tag{25}$$

Since we are considering zero spin viscosities in the angular momentum equation, the spin velocity field, $\bar{\omega} = \omega_x \bar{i}_x$, again follows the "free-to-spin" condition at the boundaries while we apply the no-slip BC, $\bar{v} = 0$, at $z = 0$ and h on the velocity field, $\bar{v} = u_y(z)\,\bar{i}_y$. Yet, for a Poiseuille geometry, the spin velocity is no longer a constant throughout the flow field, *i.e.*, $\bar{\omega} = \omega_x(z)\,\bar{i}_x$, and thus an approximate condition for the spin velocity field, namely, $\bar{\omega} \to 0$ and $\bar{\Omega} \to 0$, is needed as $z \to h/2$ [22] in order to satisfy the symmetry requirements, additional to the stability and "free-to-spin" conditions, of the spin velocity field as will be discussed in the next subsection.

B. Solutions to the Velocity Profile, Spin Velocity Profile, and the Volume Flow Rate

Following a similar procedure to that of the Couette geometry case, we integrate (37) to have

$$\Gamma z + 2\zeta\omega_x + \eta_e \frac{du_y}{dz} = C_p , \tag{38}$$

where C_p is a constant. Equation (38) is then substituted into (25) so that the angular momentum equation becomes

$$\frac{\alpha^* - \tau_{MW}\omega_x}{1 + \tau_{MW}^2 \omega_x^2} n\alpha_z E_0^2 + 2\zeta \left(\frac{\Gamma}{\eta_e} z + \frac{2\zeta}{\eta_e}\omega_x - \frac{C_p}{\eta_e} - 2\omega_x \right) = 0 . \tag{39}$$

Recall that in order to satisfy the particle and ER fluid stable rotation condition as discussed in Section III.B, the suspended micro-particles [7]-[12] and subsequently the ER fluid need to rotate in the direction of the macroscale flow vorticity, which in this case, should be the Poiseuille flow vorticity direction. Based upon this argument and with reference to the coordinate system shown in Fig. 5, it is argued that the particle rotation, Ω, and the subsequent fluid spin, ω_x, directions in the lower half of the channel, i.e., $0 \le z < h/2$, are to be clockwise or pointing into the plane (negative). As for the other half of the channel, *i.e.*, $h/2 < z \le h$, the directions of the particle rotation, Ω, and fluid spin velocity, ω_x, are required to be counter clockwise or pointing out of the plane (positive). Hence, the plane "$z = h/2$" becomes a plane of symmetry, and the ER fluid spin velocity and particle rotation goes to zero, that is, $\omega_x \to 0$ and $\Omega \to 0$ as $z \to h/2$, in this symmetry plane [22]. For simplicity, we shall denote this symmetry condition as $\bar{\omega} = \omega_x \bar{i}_x = 0$ and $\bar{\Omega} = \Omega \bar{i}_x = 0$ at $z = h/2$ henceforward. By applying this symmetry condition to (39), the constant C_p is determined to be $\Gamma h/2$, and (39) is rewritten as

$$\frac{\alpha^* - \tau_{MW}\omega_x}{1 + \tau_{MW}^2 \omega_x^2} \frac{n\alpha_z E_0^2}{2\zeta} + \frac{\Gamma h}{\eta_e}\left(\frac{z}{h} - \frac{1}{2} \right) - \frac{2\eta}{\eta_e}\omega_x = 0 , \tag{40}$$

which is an algebraic, cubic equation with the *z*-coordinate being a spatially varying coefficient and $\alpha^* = \alpha_y / \alpha_z$.

Using the following non-dimensionalization scheme, namely,

$$\omega^* = \tau_{MW}\omega_x ,\ z^* = \frac{z}{h} ,\ m^* = \frac{2\zeta\eta}{n\alpha_z E_0^2 \tau_{MW}\eta_e} , \text{ and } V^* = \frac{\Gamma h \tau_{MW}}{\eta} m^* , \tag{41}$$

(40) is non-dimensionalized and the dimensionless angular momentum equation for the Poiseuille case becomes

$$\omega^{*3} - \frac{V^*}{2m^*}\left(z^* - \frac{1}{2} \right)\omega^{*2} + \left(1 + \frac{1}{2m^*} \right)\omega^* - \frac{V^*}{2m^*}\left(z^* - \frac{1}{2} \right) - \frac{\alpha^*}{2m^*} = 0 . \tag{42}$$

We solve (42) by standard symbolic calculation packages (Mathematica, Wolfram Research, Inc.) to express ω^* in terms of V^*, z^*, and m^*, or equivalently, to express ω_x in terms of z, Γ, and E_0. Next, the stability, symmetry, and "free-to-spin" conditions are applied to rule out the most physically meaningful solution to the spin velocity, ω^*, out of the three possible solutions found from solving the angular momentum equation, (42). According to the stability and symmetry conditions as discussed previously, the spin velocity and particle rotation need to be positive in $0.5 < z^* \le 1$, negative in $0 \le z^* < 0.5$, and zero at $z^* = 0.5$ with $z^* = z/h$. From this reasoning, the explicit expression of the final solution to the spin velocity of Poiseuille flow with internal particle electrorotation is given for $E_0 \ge E_c$ as (solved by Mathematica

under "Solve" command): (i) for $0.5 < z^* \le 1$, we pick positive Ω in (15) and substitute into (17) and (23) to have

$$\omega_{P1}^* = \frac{2V^*z^* - V^*}{12m^*} + \varphi_{P1}\left[6\sqrt[3]{4}m^*\left(\varphi_{P2} + \sqrt{\varphi_{P2}^2 + 4\varphi_{P1}^3}\right)^{1/3}\right]^{-1} - \frac{1}{12\sqrt[3]{2}m^*}\left(\varphi_{P2} + \sqrt{\varphi_{P2}^2 + 4\varphi_{P1}^3}\right)^{1/3}, \tag{43}$$

(ii) for $z^* = 0.5$,

$$\omega_{P3}^* = 0 \ (\Omega = 0), \tag{44}$$

and (iii) for $0 \le z^* < 0.5$, we pick negative Ω in (15) and have

$$\omega_{P2}^* = \frac{2V^*z^* - V^*}{12m^*} - \varphi_{P1}\left(1 + i\sqrt{3}\right)\left[12\sqrt[3]{4}m^*\left(\varphi_{P2} + \sqrt{\varphi_{P2}^2 + 4\varphi_{P1}^3}\right)^{1/3}\right]^{-1} + \frac{1}{24\sqrt[3]{2}m^*}\left[\left(1 - i\sqrt{3}\right)\left(\varphi_{P2} + \sqrt{\varphi_{P2}^2 + 4\varphi_{P1}^3}\right)^{1/3}\right], \tag{45}$$

where

$$\varphi_{P1} = 24m^*\left(1 + 2m^*\right) - \left(2V^*z^* - V^*\right)^2, \tag{46}$$

and

$$\varphi_{P2} = -72m^*V^* + 288m^{*2}V^* + 2V^{*3} + 144m^*V^*z^* - 576m^{*2}V^*z^* - 12V^{*3}z^* + 24V^{*3}z^{*2} - 16V^{*3}z^{*3} - 864m^{*2}\alpha^*. \tag{47}$$

Notice that the solution given to (42) should always be real valued within our parametric range of interest since there is generally no physical meaning for a solution being complex valued. Moreover, the combination of solutions, *i.e.*, (43), (44), and (45), presented herein is for the general parametric range of electric field strengths $E^* = E_0/E_c \ge 1$. For other parametric regimes, the combination of solutions *may be* different from the one presented herein, *e.g.*, (43) is generally uniformly valid for the case of $E_0 < E_c$ throughout $0 \le z^* \le 1$ (with $\Omega = 0$ in (17) and (23)). In this latter case, we need to start from (42) and solve for the three roots, then apply the stability, symmetry, and "free-to-spin" conditions to the solutions, and finally rule out the suitable combination for the desired spin velocity field just as the procedure we have shown to find the combination of (43), (44), and (45). Also notice that the jump or discontinuity made in the final spin velocity profile at $z^* = 0.5$ is permitted self-consistently by the "free-to-spin" condition for the zero spin viscosity cases studied herein. This is an analogous situation to the "inviscid" parallel shear flow with the *velocity field* being $\bar{v} = U\bar{i}_y$ for $z > 0$ and $\bar{v} = -U\bar{i}_y$ for $z < 0$ as one of the possible base solutions to Kelvin-Helmholtz instability studies.

Having (43), (44), and (45) combined, we can easily express the dimensional spin velocity in either $\omega_x = \omega_x(z)$ or $\omega_x = \omega_x(z^*)$ forms by dividing ω^* with the Maxwell-Wagner time, τ_{MW}. After substituting ω_x and $C_p = \Gamma h/2$ into (38) and also noticing that ω_x, for $E^* \ge 1$, is expressed by (43) and (45) in the respective regions of $0.5 < z^* \le 1$ and $0 \le z^* < 0.5$, we integrate (38) with respect to z to obtain the velocity field as: (i) for $0.5 < z^* \le 1$,

$$u_{UP}^*(z^*) = \frac{\eta}{\eta_e}\left[z^*(1 - z^*) + \frac{4\zeta}{\Gamma h\tau_{MW}}\int_{z^*}^1 \omega_{P1}^*\left(\widehat{z^*}\right)d\widehat{z^*}\right], \tag{48a}$$

and (ii) for $0 \le z^* < 0.5$,

$$u_{DN}^*(z^*) = \frac{\eta}{\eta_e}\left[z^*(1 - z^*) - \frac{4\zeta}{\Gamma h\tau_{MW}}\int_0^{z^*} \omega_{P2}^*\left(\widehat{z^*}\right)d\widehat{z^*}\right], \tag{48b}$$

where the velocity field, (48), is made dimensionless by dividing both (48a) and (48b) with $\Gamma h^2/2\eta$ (*note*: use η not η_e), *i.e.*, $u^*(z^*) = 2\eta u_y(z^*)/\Gamma h^2$, ω_{P1}^* and ω_{P2}^* are respectively defined in (43) and (45), and $\widehat{z^*}$ is a dummy index in both equations (for $E^* < 1$ use ω_{P1}^* throughout $0 \le z^* \le 1$ in the integration of (48)). From both mathematical and physical point of views, the velocity field or distribution of the flow, u_y, needs to be continuous and smooth (continuous in du_y/dz) throughout the channel because of finite ER fluid viscosities, η. However, since we have manually (with physical reasoning) made the spin velocity, ω_x, discontinuous at the middle of the channel, the smoothness of the velocity distribution near $z^* = 0.5$ may not exactly be preserved under the framework of zero spin viscosity limits—a cusp may arise at $z^* = 0.5$ in the velocity profile given by (48) for certain parametric regimes of interest. The velocity and spin velocity profiles for the Poiseuille geometry found in this subsection will be evaluated numerically and presented graphically in Section IV.C to further illustrate these issues.

We next calculate the two dimensional volumetric flow rate, Q, by integrating the velocity fields, *i.e.*,

$$Q = \int_0^h u_y(z)dz = \frac{\Gamma h^3}{2\eta}\left[\int_0^{0.5} u_{DN}^*(z^*)dz^* + \int_{0.5}^1 u_{UP}^*(z^*)dz^*\right], \tag{49}$$

with (48a) used for $0.5 < z^* \le 1$ and (48b) used for $0 \le z^* < 0.5$. In terms of the spin velocities, (49) is rewritten as

$$Q = \left(\frac{\Gamma h^3}{12\eta}\right)\left(\frac{\eta}{\eta_e}\right)\times \left\{1 + \frac{24\zeta}{\Gamma h\tau_{MW}}\left[\int_{0.5}^1\int_{z^*}^1 \omega_{P1}^*\left(\widehat{z^*}\right)d\widehat{z^*}dz^* - \int_0^{0.5}\int_0^{z^*} \omega_{P2}^*\left(\widehat{z^*}\right)d\widehat{z^*}dz^*\right]\right\}, \tag{50}$$

where $\widehat{z^*}$ is the dummy index and (43) and (45) are used in the integration ranges of $0.5 < z^* \le 1$ and $0 \le z^* < 0.5$, respectively. Again, for $E^* < 1$, use ω_{P1}^* throughout $0 \le z^* \le 1$ in the integration of (49) or (50). It is now obvious why we use η, ER fluid viscosity when no electric field is applied, instead of $\eta_e = \eta + \zeta$ in non-dimensionalizing the velocity field of (48). The intention is to utilize the ordinary Poiseuille flow solution (no electric field applied to the ER fluid) as a reference datum so that the variation and deviation of the electrorotation modified Poiseuille velocities and flow rates from those of the zero electric field solution, *i.e.*, $u_0^*(z^*) = (2\eta/\Gamma h^2)u_y(z^*) = z^*(1 - z^*)$ and $Q_0 = \Gamma h^3/12\eta$, respectively, can be clearly and effectively compared.

Results of the velocity/spin velocity profiles and the volume flow rate will be respectively presented in the following subsection. The system parameters, physical constants, and material properties used in the numeric evaluations can be found in Table II unless otherwise specified.

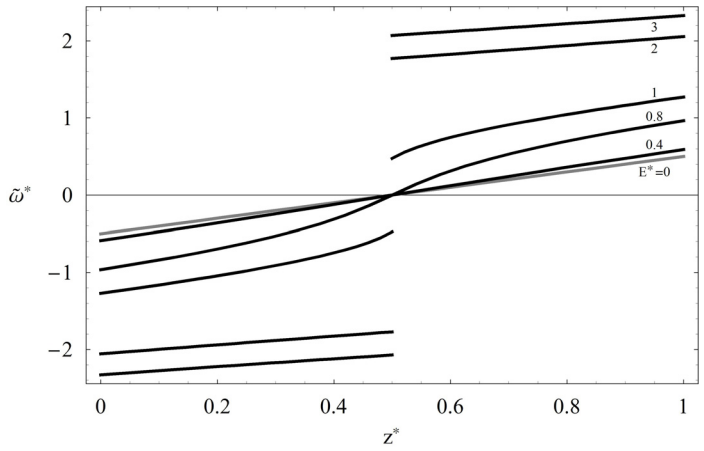

FIG. 6. The Poiseuille spin velocity profile (normalized), $\widetilde{\omega^*}$, plotted with respect to the spatial coordinate, z^*, evaluated at $E^* = 0$, 0.4, 0.8, 1.0, 2.0, and 3.0, with $\Gamma^* = 1$. The gray curve denotes the zero electric field value for the spin velocity, i.e., the vorticity of ordinary Poiseuille flow. For $E^* \geq 1$, (43)-(45) are used in the evaluation, whereas for $E^* < 1$, (43) is used throughout the spatial domain of interest.

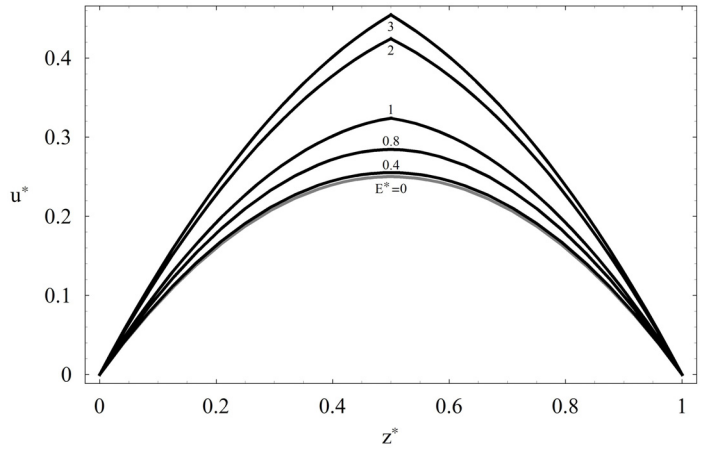

FIG. 7. The linear velocity profile (normalized), u^*, of Poiseuille flow with internal micro-particle electrorotation plotted with respect to the spatial coordinate, z^*, evaluated at $E^* = 0$, 0.4, 0.8, 1.0, 2.0, and 3.0, with $\Gamma^* = 1$. The gray curve denotes the zero electric field value for the velocity profile, which is the original Poiseuille parabolic profile. Equations (43) (*with a positive valued* Ω *from (15) used in (17) and (23)*) and (45) (*with a negative valued* Ω *from (15) used in (17) and (23)*) are respectively used in the integrals of (48a) and (48b) for $E^* \geq 1$. The evaluation for $E^* < 1$ is done by employing (43) in both (48a) and (48b).

C. *Results and Discussions*

Before presenting the spin velocity profiles, we first normalize the Poiseuille spin velocity, (43), (44), and (45) by $\Gamma h \tau_{MW}/2\eta$, namely, $\widetilde{\omega^*} = \widetilde{\omega^*_{P1}} = 2\eta\omega^*_{P1}/\Gamma h\tau_{MW}$ for $0.5 < z^* \leq 1$, $\widetilde{\omega^*} = \widetilde{\omega^*_{P2}} = 2\eta\omega^*_{P2}/\Gamma h\tau_{MW}$ for $0 \leq z^* < 0.5$, and $\widetilde{\omega^*} = \widetilde{\omega^*_{P3}} = 2\eta\omega^*_{P3}/\Gamma h\tau_{MW} = 0$ for $z^* = 0.5$. By employing this normalization, we find that the zero electric field solution, $\omega^*_0 = \Gamma h\tau_{MW}\left(z^* - 0.5\right)/2\eta$, becomes independent of the applied pressure gradient and only depends on the spatial position in the channel, *i.e.*, $\widetilde{\omega^*_0} = \left(z^* - 0.5\right)$. The zero electric field solution then becomes a reference datum invariant of both the applied electric field strength and the driving pressure gradient and facilitates a more physically meaningful comparison among the solutions.

Illustrated in Fig. 6 are the spatial variations of the electrorotation assisted Poiseuille spin velocity profiles given by (43), (44), and (45) normalized by $\Gamma h\tau_{MW}/2\eta$ plotted with respect to distinct strengths of the applied electric field, $E^* = E_0/E_c$. With the pressure gradient kept constant, *i.e.*, $\Gamma^* = \Gamma/\Gamma_r = 1$ where $\Gamma_r = 2\times10^4$ $(Pa\cdot m^{-1})$, the normalized spin velocity $\widetilde{\omega^*}$ is evaluated at $E^* = 0$, 0.4, 0.8, 1.0, 2.0, and 3.0 with $E_c = 1.3\times10^6$ (Vm^{-1}). The solid gray curve shown in Fig. 6 represent the zero electric field solution, $\widetilde{\omega^*_0} = \left(z^* - 0.5\right)$, or half of the Poiseuille vorticity when there is no electric field and internal particle electrorotation effects. From the figure, the positive and negative valued spin velocities found in the respective regions of $0.5 < z^* \leq 1$ and $0 \leq z^* < 0.5$ (with $\widetilde{\omega^*} = \widetilde{\omega^*_{P3}} = 0$ at $z^* = 0.5$) again verify that we have chosen, based on the macro Poiseuille vorticity directions, the combination of solutions that satisfies the symmetry as well as the stable particle and ER fluid rotation conditions. The apparent jump or discontinuity in the spin velocity profile at $z^* = 0.5$ is self-consistently permitted by the "free-to-spin" condition under the framework of the zero spin viscosity limit as already mentioned in the previous sections.

As can be seen in Fig. 6, the magnitude of the normalized spin velocity of Poiseuille flow with internal particle electrorotation increases as the applied DC electric field strength is increased. If, on the contrary, we reduce the applied electric field strength from $E^* = 1.0$, 0.8 to 0.4, we find that the spin velocity gradually approaches the zero electric field solution noted by the gray curve in Fig. 6. Moreover, the strength of the jump or discontinuity at $z^* = 0.5$ in the normalized spin velocity field reduces and eventually smoothes out (see the smooth and continuous curves for $E^* = 0.4$ and 0.8) as the applied electric field is decreased. Note that in this figure, the solutions for $E^* = 0.4$ and 0.8 are fully represented by $\widetilde{\omega^*} = \widetilde{\omega^*_{P1}}$, *i.e.*, (43), throughout the spatial domain, $0 \leq z^* \leq 1$, at $\Gamma^* = 1$. However, the spin velocity solutions for $E^* = 1.0$, 2.0, and 3.0 are represented by $\widetilde{\omega^*} = \widetilde{\omega^*_{P1}}$ for $0.5 < z^* \leq 1$, $\widetilde{\omega^*} = \widetilde{\omega^*_{P2}}$ for $0 \leq z^* < 0.5$, and zero for $z^* = 0.5$ at $\Gamma^* = 1$. The transition among the braches of solutions again verifies the cubic nature of the governing equation, (42).

After the spin velocity field is found, the (linear) velocity field is easily obtained by integrating (48). The results of the velocity field, u^* (or u_y), are plotted with respect to the spatial coordinate z^* in Fig. 7 for $\Gamma^* = 1$ with $E^* = 0$, 0.4, 0.8, 1.0, 2.0, and 3.0. The gray solid curve represent the zero electric field solution, $u^*_0 = z^*\left(1 - z^*\right)$, *i.e.*, the velocity field of ordinary Poiseuille flow without internal particle electrorotation. Recall that the velocity field was already normalized by $\Gamma h^2/2\eta$ in the non-dimensional definition of (48); hence, there is no more need to define a normalized velocity field as in the case of the spin velocity.

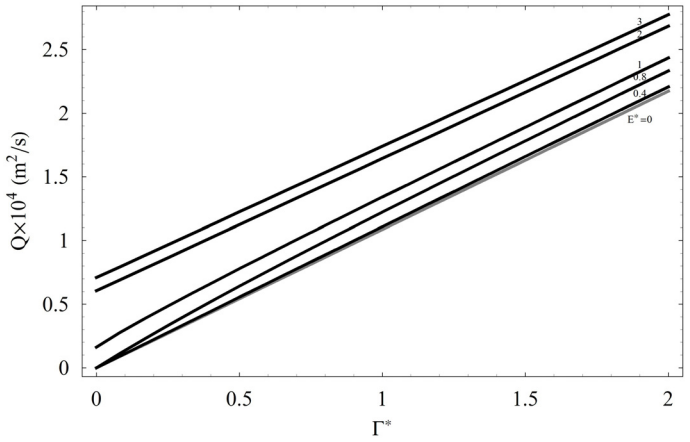

FIG. 8. The two dimensional Poiseuille volume flow rate, Q, plotted with respect to the applied pressure gradient, Γ^*, evaluated at $E^* = 0$, 0.4, 0.8, 1.0, 2.0, and 3.0. The gray curve represents the zero electric field volume flow rate given by $Q_0 = \Gamma h^3/12\eta$.

Based upon the above convention, we find in Fig. 7 that with $\Gamma^* = 1$ kept constant, the flow velocity is considerably enhanced and the cusp in the velocity profile at $z^* = 0.5$ is sharpened as the strength of the applied DC electric field is increased. If we reduce the strength of the electric field while the pressure gradient is maintained constant, the cusp at $z^* = 0.5$ becomes blunt and the electrorotation enhanced velocity profile gradually reduces and converges back to the $E^* = 0$ solution, *i.e.*, the parabolic Poiseuille flow velocity field without internal particle electrorotation as noted by the solid gray curve in the figure. The $E^* = 0.4$ and 0.8 velocity fields shown is evaluated by substituting (43), *i.e.*, ω_{P1}^*, into the integrals of both (48a) and (48b) with $\Omega = 0$ in (17) and (23) since in this parametric regime, ω_{P1}^* assumes a real value and is uniformly valid throughout the spatial domain of $0 \le z^* \le 1$. The cusped velocity profile shown in Fig. 7 is similar to the velocity profiles of a power law fluid in circular pipe Poiseuille flow geometries for large power indices [42].

Finally, using the physical parameters and material properties given in Table II, the two dimensional volume flow rate of Poiseuille flow with internal particle electrorotation, Q ($m^2 s^{-1}$), is plotted with respect to the driving pressure gradient, $\Gamma^* = \Gamma/\Gamma_r$ with $\Gamma_r = 2\times10^4$ ($Pa\cdot m^{-1}$), at distinct values of the applied DC electric field strength, $E^* = E_0/E_c$ with $E_c = 1.3\times10^6$ (Vm^{-1}). The results are shown in Fig. 8 for $E^* = 0$, 0.4, 0.8, 1.0, 2.0, and 3.0 with the solid gray curve noted by $E^* = 0$ corresponding to the two dimensional volume flow rate of Poiseuille flow without internal particle electrorotation, *i.e.*, $Q_0 = \Gamma h^3/12\eta$.

From Fig. 8, we find that the volume flow rate increases as the applied DC electric field strength is increased while the driving pressure gradient is kept constant. On the other hand, the eletrorotation enhanced volume flow rate gradually converges back to the zero electric field solution, $Q_0 = \Gamma h^3/12\eta$, as the applied electric field is reduced. These results are consistent with our previous examination of the velocity fields shown in Fig. 7 and agree with the experimental observations reported in [10]. Note that the flow rate solutions for $E^* =$ 1.0, 2.0, and 3.0 suggest a non-zero flow rate at zero driving pressure gradients when the flow is subjected to an applied electric field larger than or equal to the critical electric field for the onset of Quincke rotation. This result is particularly due to the fact that we have used the combination of solutions of the spin velocity, (43), (44), and (45), that rotates in the same direction as the macroscale Poiseuille flow vorticity field in the modeling and evaluation of the volume flow rate, Q. Nonetheless we need to pointed out that unless there is some initial flow ($\Gamma^* \neq 0$) applied to give the suspended micro-particles and subsequently the ER fluid a favorable direction for electrorotation, the direction for Quincke rotation is merely a matter of chance with the particle rotation axis either pointing into or out of the planes defined by the electric field under zero flow or equivalently zero driving pressure gradient conditions. Up to this point, no experimental evidence has observed a finite flow rate for the ER fluid when $E_0 > E_c$ and the pressure gradient being zero [7]. This finite jump of volume flow rate at zero driving pressure gradients diminishes and eventually becomes zero, *i.e.*, zero flow rate at zero pressure gradient, as we reduce the applied electric field strength from $E^* =$ 1.0, 0.8, to 0.4 as can be found in the figure. Again, for the $E^* = 0.4$ and 0.8 solutions shown in Fig. 8, we have used ω_{P1}^* throughout the spatial domain, $0 \le z^* \le 1$.

Last, we can compare the theoretical predictions of the 2D Poiseuille volume flow rate obtained from the present continuum model with the results given in Figs. 5 and 6 of Lemaire *et al.* [10]. By using the same material and physical parameters employed in [10], *e.g.*, channel height $h = 750$ (μm), electric field strengths of $E_0 = 2700$ and 3300 ($V\cdot mm^{-1}$), solid volume fractions of $\phi = 0.05$ and 0.1, etc., it can be found that the variation of the 2D volume flow rate with respect to E^* and Γ^* predicted by the continuum model is similar to the predicted results obtained from models based on single particle dynamics given in [10]—the volume flow rate increases as the applied electric field increases. However, results from the present continuum analysis slightly over estimates the volume flow rate as compared to both experimental data and predictions single particle dynamics analysis.

Summing up the findings from examining Figs. 6, 7 and 8, it is found that, in general, the magnitude of the normalized spin velocity, the normalized flow velocity, and the 2D volume flow rate is increased as the applied electric field, E^*, is increased with the driving pressure gradient, Γ^*, kept constant. Moreover, increasing the applied electric field gives rise to a more severe jump or discontinuity at $z^* = 0.5$ in the normalized spin velocity profile, sharpens the cusp structure at $z^* = 0.5$ in the (normalized) velocity profile, and results in a finite value of volume flow at zero pressure gradients. Contrarily, reducing the strength of the electric field smoothes out the cusp in the velocity profile and reduces the severity of the discontinuity at $z^* = 0.5$ in the spin velocity field while the pressure gradient is kept constant. The (normalized) velocity and spin velocity profiles as well as the 2D volume flow rate gradually converge back to the zero electric field solutions as the applied electric field strength is reduced.

As a general conclusion of the results presented herein, we find that the fully continuum governing equations describing the internal particle electrorotation modified flow phenomena employed in this article reduces to a "particulate limit" and predicts similar trends of variation of the effective viscosities for Couette flow and the two dimensional volume flow rates for Poiseuille flow as compared to the theoretic predictions from two-phase effective continuum (single particle dynamics based) models found in the literature when the spin viscosity, η', is set to be zero in the angular momentum equations.

V. CONCLUDING REMARKS

Two dimensional Couette and Poiseuille flows with internal, spontaneous micro-particle electrorotation, or Quincke rotation, are modeled and analyzed through a fully continuum mechanical formulation in this article. By combining the theories of particle electromechanics and anti-symmetric stresses, general governing equations are given to describe the physical aspects of polarization relaxation, mass conservation, momentum conservation, and angular momentum conservation involved in this novel electrorheological phenomena. With the assumptions of steady, incompressible, fully developed, and two dimensional flow, the general governing equations are respectively reduced to two algebraic, cubic equations of the ER fluid spin velocity, ω^*, for both Couette and Poiseuille geometries under the framework of a zero spin viscosity in the angular momentum equations. Stability, symmetry, and "free-to-spin" conditions are then applied to the cubic spin velocity equations to rule out the solution or combination of solutions consistent with the physical assumptions and phenomena of interest. Expressions of the linear velocity field, u^*, and effective viscosity, η^*, for Couette flow as well as the linear velocity and volume flow rate, Q, for Poiseuille flow can be further derived in terms of the applied electric field, E^*, shear rate, γ^*, driving pressure gradient, Γ^*, or spatial coordinate, z^*, by respectively substituting the most physically suitable and meaningful solution or combination of solutions to the spin velocity into the linear momentum equation with the no-slip boundary conditions on the velocity field applied at the spatial boundaries. The results are summarized in the following:

(i) With internal particle electrorotation, the spin velocity, ω^*, increases as either the applied electric field strength, E^*, or the shear rate, γ^*, is increased for Couette flow. Contrarily, the spin velocity reduces back to the zero electric field solution ($E^* = 0$, no particle electrorotation), *i.e.*, $\omega_0^* = -\gamma^*/2$, or half of the Couette flow vorticity, as the applied electric field strength is decreased. In the limit of zero spin viscosities, the linear Couette velocity profile, $u_y(z) = U_0 z/h$, remains invariant regardless of the applied electric field strength.

(ii) The effective viscosity, η^*, is found to decrease as the applied DC electric field strength increases for Couette flow with internal particle electrorotation. However, as the driving shear rate grows large, the amount of reduction in the effective viscosity is reduced regardless of the applied electric field strength. For a decreasing electric field strength, the effective viscosity converges back to the zero electric field solution, $\eta^* = 1$, *i.e.*, the viscosity of the ER fluid (particle-liquid mixture) when no electric field is applied.

(iii) With a constant driving pressure gradient, Γ^*, the magnitude of the normalized Poiseuille spin velocity, $\widetilde{\omega^*}$, as well as the jump or discontinuity in the spin velocity profile increases as the applied electric field, E^*, increases whereas the spin velocity reduces back to the zero field solution, $\widetilde{\omega_0^*} = \left(z^* - 0.5\right)$, and the discontinuity in the spin velocity profile diminishes as E^* is reduced.

(iv) With a constant driving pressure gradient, Γ^*, the magnitude of the dimensionless (normalized) Poiseuille linear velocity, u^*, as well as the sharpness of the cusp in the velocity profile increases as the applied electric field, E^*, increases. On the contrary, the velocity profile reduces back to the zero field solution, $u_0^* = z^*\left(1 - z^*\right)$, and the cusp in the velocity profile becomes blunt as E^* is reduced.

(v) The two dimensional Poiseuille volume flow rate, Q, increases as the applied DC electric field strength increases whereas the electrorotation enhanced flow rate solution reduces back to the zero electric field solution, $Q_0 = \Gamma h^3/12\eta$, as the applied electric field is decreased. At zero driving pressure gradients, the electrorotation enhanced volume flow rate assumes some finite value because of the fact that we have employed the spin velocity solution that rotates in the same direction as that of the Poiseuille vorticity field in the evaluation of Q.

(vi) Comparing the results of effective viscosity and volume flow rate obtained herein with those found in current literature, we find that both continuum and semi-continuum (single particle dynamics based) models qualitatively predict the same trends of variation for the effective viscosity with respect to the electric field strength and average shear rate, and for the volume flow rate with respect to the field strength and driving pressure gradient.

Future work includes a more advanced modeling of the polarization relaxation processes in the electrorheological fluid flow, the investigation of finite spin viscosity effects on the angular momentum balances within the flow field, and the search of possible practical applications for such novel negative electrorheological phenomenon.

REFERENCES

[1] W.M. Winslow, "Induced fibration of suspensions," *Journal of Applied Physics*, Vol. 20, pp.1137-1140, 1949.

[2] T.C. Halsey, "Electrorheological fluids," *Science*, Vol. 258(5083), pp.761-766, 1992.

[3] D.J. Klingenberg and C.F. Zukoski IV, "Studies of the steady-shear behavior of electrorheological suspensions," *Langmuir*, Vol. 6, pp.15-24, 1990.

[4] J.N. Foulc, N. Felici, and P. Atten, "Interpretation of electrorheological effect," *Comptes Rendus de l'Academie des Sciences*, *Serie II*, Vol. 314(12), pp.1279-1283, 1992.

[5] C. Boissy, P. Atten, and J.N. Foulc, "On a negative electrorheological effect," *Journal of Electrostatics*, Vol. 35, pp.13-20, 1995.

[6] C.W. Wu and H. Conrad, "Negative electrorheological effect and electrical properties of a Teflon/silicone oil suspension," *Journal of Rheology*, Vol. 41(2), pp.267-281, 1997.
[7] L. Lobry and E. Lemaire, "Viscosity decrease induced by a DC electric field in a suspension," *Journal of Electrostatics*, Vol. 47, pp.61-69, 1999.
[8] A. Cebers, E. Lemaire, and L. Lobry, "Internal rotations in dielectric suspensions," *Magnetohydrodynamics*, Vol. 36(4), pp.347-364, 2000.
[9] A. Cebers, E. Lemaire, and L. Lobry, "Flow modification induced by Quincke rotation in a capillary," *International Journal of Modern Physics B*, Vol. 16(17-18), pp.2063-2069, 2002.
[10] E. Lemaire, L. Lobry, and N. Pannacci, "Flow rate increased by electrorotation in a capillary," *Journal of Electrostatics*, Vol. 64, pp.586-590, 2006.
[11] N. Pannacci, E. Lemaire, and L. Lobry, "Rheology and structure of a suspension of particles subjected to Quincke rotation," *Rheologica Acta*, Vol. 46, pp.899-904, 2007.
[12] E. Lemaire, L. Lobry, N. Pannacci, and F. Peters, "Viscosity of an electro-rheological suspension with internal rotations," *Journal of Rheology*, Vol. 52(3), pp.769-783, 2008.
[13] G. Quincke, "Ueber rotationen im constanten electrischen felde," *Annalen der Physik und Chemie*, Band 59(11), pp.417-486, 1896.
[14] J.R. Melcher and G.I. Taylor, "Electrohydrodynamics: a review of the role of interfacial shear stresses," *Annual Review of Fluid Mechanics*, Vol. 1, pp.111-146, 1969.
[15] J.R. Melcher, "Electric fields and moving media," *IEEE Transactions on Education*, Vol. E-17(2), pp.100-110, 1974.
[16] J.R. Melcher, *Continuum Electromechanics*, Cambridge, MA: The MIT Press, 1981, pp.5.49-5.54.
[17] T.B. Jones, "Quincke rotation of spheres," *IEEE Transactions on Industry Applications*, Vol. IA-20(4), pp.845-849, 1984.
[18] T.B. Jones, *Electromechanics of Particles*, New York, NY: Cambridge University Press, 1995, pp.83-109, 175-177.
[19] R. Moskowitz and R.E. Rosensweig, "Nonmechanical torque- driven flow of a ferromagnetic fluid by an electromagnetic field," *Applied Physics Letters*, Vol. 11(10), pp.301-303, 1967.
[20] R.E. Rosensweig, J. Popplewell, and R.J. Johnston, "Magnetic fluid motion in rotating field," *Journal of Magnetism and Magnetic Materials*, Vol. 85, pp.171-180, 1990.
[21] R.E. Rosensweig, *Ferrohydrodynamics* (reprint edn.), Mineola, NY: Dover Publications, 1997, pp.237-271.
[22] X. He, "Ferrohydrodynamic flows in uniform and non-uniform rotating magnetic fields," Ph.D. Dissertation, Department of Electrical Engineering and Computer Science, Massachusetts Institute of Technology, Cambridge, MA, 2006.
[23] S.M. Elborai, "Ferrofluid Surface and Volume Flows in Uniform Rotating Magnetic Fields,' Ph.D. Dissertation, Department of Electrical Engineering and Computer Science, Massachusetts Institute of Technology, Cambridge, MA, 2006.
[24] A. Chaves, C. Rinaldi, S. Elborai, X. He, and M. Zahn, "Bulk flow in ferrofluids in a uniform rotating magnetic field," *Physical Review Letters*, Vol. 96(19), 194501, 2006.
[25] A. Chaves, F. Gutman, and C. Rinaldi, "Torque and bulk flow of ferrofluid in an annular gap subjected to a rotating magnetic field," *Transactions of the ASME-Journal of Fluids Engineering*, Vol. 129, pp.412-422, 2007.
[26] A. Chaves, M. Zahn, and C. Rinaldi, "Spin-up flow of ferrofluids: asymptotic theory and experimental measurements," *Physics of Fluids*, Vol. 20(5), 053102, 2008.
[27] J.S. Dahler and L.E. Scriven, "Angular momentum of continua," *Nature*, Vol. 192, pp.36-37, 1961.
[28] D.W. Condiff and J.S. Dahler, "Fluid mechanical aspects of anti-symmetric stress," *Physics of Fluids*, Vol. 7(6), pp.842-854, 1964.
[29] A.C. Eringen, "Theory of micropolar fluids," *Journal of Mathematics and Mechanics*, Vol. 16(1), pp.1-16, 1966.
[30] K.R. Schumacher, I. Sellien, G.S. Knoke, T. Cader, and B.A. Finlayson, "Experiment and simulation of laminar and turbulent ferrofluid pipe flow in an oscillating magnetic field," *Physical Review E*, Vol. 67, 026308, 2003.
[31] S. Feng, A.L. Graham, J.R. Abbott, and H. Brenner, "Anti-symmetric stresses in suspensions: vortex viscosity and energy dissipation," *Journal of Fluid Mechanics*, Vol. 563, pp.97-122, 2006.
[32] H. Brenner, "Rheology of two-phase systems," *Annual Review of Fluid Mechanics*, Vol. 2, pp.137-176, 1970.
[33] H.A. Haus and J.R. Melcher, *Electromagnetic Fields and Energy*, Englewood Cliffs, NJ: Prentice-Hall, 1989, Chapter 3.
[34] A. O. Cebers, "Internal rotation in the hydrodynamics of weakly conducting dielectric suspensions," *Mekhanika Zhidkosti i Gaza*, Vol. 2, pp.86-93, 1980. (see also *Fluid Dynamics*, Vol. 15(2), pp.245-251, 1980.)
[35] J.J. Xiao, J.P. Huang, and K.W. Yu, "Dynamic polarizability of rotating particles in electrorheological fluids," *Journal of Physical Chemistry B*, Vol. 112, pp.6767-6771, 2008.
[36] M.I. Shliomis, "Certain gyromagnetic effect in a liquid paramagnet," *Soviet Phys. JEPT*, Vol. 39(4), pp.701-704, 1974.
[37] M.I. Shliomis, "Nonlinear effects in suspension of ferromagnetic particles under action of a rotating magnetic field," *Soviet Phys. Dokl.*, Vol. 19(10), pp.686-687, 1975.
[38] M.I. Shliomis, "Effective viscosity of magnetic suspensions," *Soviet Physics JETP*, Vol. 34(6), pp.1291-1294, 1972.
[39] M. Zahn and D.R. Greer, "Ferrohydrodynamic pumping in spatially uniform sinusoidally time-varying magnetic fields," *Journal of Magnetism and Magnetic Materials*, Vol. 149, pp.165-173, 1995.
[40] M. Zahn and L.L. Pioch, "Magnetizable fluid behavior with effective positive, zero, or negative dynamic viscosity," *Indian Journal of Engineering and Material Sciences*, Vol. 5, pp.400-410, 1998.
[41] M. Zahn and L.L. Pioch, "Ferrofluid flows in AC and traveling wave magnetic fields with effective positive, zero, or negative dynamic viscosity," *Journal of Magnetism and Magnetic Materials*, Vol. 201, pp.144-148, 1999.
[42] R.P. Chhabra and J.F. Richardson, *Non-newtonian Flow in the Process Industries: Fundamentals and Engineering Applications*, Boston, MA: Butterworth-Heinemann, 1999, Chapter 3.